AGB CONNECTION AND ULTRAVIOLET LUMINOSITY EXCESS IN ELLIPTICAL GALAXIES

Alberto Buzzoni[1] and Rosa A. González-Lópezlira[2]
Received 2007 November 13; accepted 2008 May 7

ABSTRACT

Relying on infrared surface brightness fluctuactions to trace AGB properties in a sample of elliptical galaxies in the Virgo and Fornax Clusters, we assess the puzzling origin of the "UV upturn" phenomenon, recently traced to the presence of a hot horizontal branch (HB) stellar component. The UV upturn actually signals a profound change in the galaxy stellar populations, involving both the hot stellar component and red giant evolution. In particular, the strengthening of the UV rising branch is always seen to correspond to a shortening in AGB deployment; this trend can be readily interpreted as an age effect, perhaps mildly modulated by metal abundance. Brightest stars in ellipticals are all found to be genuine AGB members, all the way, and with the AGB tip exceeding the RGB tip by some $0.5-1.5$ mag. The inferred core mass of these stars is found to be $\lesssim 0.57\,M_\odot$ among giant ellipticals. This value accounts for the recognized deficiency of planetary nebulae in these galaxies, as a result of a lengthy transition time for the post-AGB stellar core to become a hard UV emitter and eventually "fire up" the nebula. The combined study of galaxy $(1550 - V)_0$ color and integrated $H\beta$ index points to a a bimodal temperature distribution for the HB with both a red clump and an extremely blue component, in a relative proportion $[N(\mathrm{RHB}):N(\mathrm{BHB})] \sim [80:20]$. For the BHB stellar population, $[\mathrm{Fe/H}]$ values of either $\simeq -0.7$ or $\gtrsim +0.5$ dex may provide the optimum ranges to feed the needed low-mass stars $(M_* \ll 0.58\,M_\odot)$ that at some stage begin to join the standard red clump stars.

Subject headings: galaxies: elliptical and lenticular, cD — galaxies: evolution — stars: AGB and post-AGB — stars: mass loss — ultraviolet: galaxies

Online material: color figures

1. INTRODUCTION AND THEORETICAL FRAMEWORK

The so-called UV upturn phenomenon (Code & Welch 1979), i.e., the rising ultraviolet emission shortward of 2000 Å, sometimes featuring in the spectral energy distribution (SED) of elliptical galaxies and the bulges of spirals, has long been a puzzling problem for old galaxy environments dominated by stars of mass comparable to the Sun.

In fact, the implied existence of an important contribution of (long-lived) B stars, hotter than $\sim 30{,}000$ K and providing up to about 2% of the galaxy bolometric luminosity (Renzini & Buzzoni 1986), has been alternately identified with different evolutionary stages. Such stages include binaries (Brown et al. 2006), blue stragglers (Bailyn 1995), blue horizontal-branch (HB) stars (Dorman et al. 1995), asymptotic giant branch (AGB) manqué stars (Greggio & Renzini 1990), and post-AGB nuclei of planetary nebulae (PNe; Renzini & Buzzoni 1986; see O'Connell [1999] for an exhaustive review, and a more recent update by Yi & Yoon [2004]).

Resolved color-magnitude diagrams (CMDs) of stellar populations in M32 (Brown et al. 1998, 2000) have definitely shown that even its relatively poor UV emission almost entirely arises from a fraction of hot HB stars, further complemented by a minority contribution from post-AGB PN nuclei. Still, facing the established interpretative scenario, one is left with at least three important issues that need to be assessed to understand the real nature of the UV upturn phenomenon:

1. The canonical evolutionary framework experienced in Galactic globular clusters naturally predicts a blue HB morphology only for old, metal-poor stellar populations (Chiosi et al. 1992; Renzini & Fusi Pecci 1988). If this is the case for ellipticals too,

then UV stars should represent the $Z \ll Z_\odot$ tail of a (supposedly) broad metallicity distribution seen to peak at much higher values, around solar abundance. Clearly, a more composite picture might be envisaged once one admits nonstandard models (i.e., including the effects of stellar rotation, helium mixing, differential mass loss, etc.) to account, in particular, for the well-known "second parameter" dilemma (Sweigart 1997; Buonanno et al. 1997; Catelan et al. 2001; Recio-Blanco et al. 2006). However, this unconventional approach still suffers from a somewhat arbitrary fine-tuning of the key physical assumptions.

2. Hot HB stars might, nonetheless, also be naturally predicted among super metal-rich stellar models, as far as metal abundance (and the linked helium content) exceeds some critical threshold. Presumably, in this case mass loss allows stars to reach the HB phase with a conveniently low external envelope, compared to the helium core mass (Dorman et al. 1993; Castellani et al. 1992; Yi et al. 1998; Buzzoni 1995; D'Cruz et al. 1996). Such "extreme HB" stars (EHB) have actually been observed, for example, in ω Cen (D'Cruz et al. 2000), NGC 6388 and NGC 6441 (Rich et al. 1997), and in some old Galactic open clusters as well, like NGC 6791 (Kaluzny & Udalski 1992; Buson et al. 2006). They clearly remain the favorite candidates to explain the evolutionary framework of UV-enhanced elliptical galaxies (Busso et al. 2005).

This hypothesis implies, however, a direct relationship between chemical abundance (modulating the helium core mass at the HB onset) and mass-loss efficiency (to suitably "peel off" the stellar envelope along the RGB). As a consequence, one has to expect the UV-to-optical color to be, eventually, one of the most quickly evolving features in the SED of elliptical galaxies (Park & Lee 1997). In theory, the UV upturn can fade by several magnitudes as the look-back time increases by a few Gyr, although the effect is still detectable at intermediate redshift ($z \sim 0.3$; Brown et al. 2003; Ree et al. 2006). Unfortunately, the evolutionary details are extremely model-dependent, and a strong UV excess could

[1] INAF-Osservatorio Astronomico di Bologna, Via Ranzani 1, 40127 Bologna, Italy.
[2] Centro de Radioastronomía y Astrofísica, Universidad Nacional Autónoma de México, 58190 Morelia, Michoacán, Mexico.

be triggered at ages as early as ~6 Gyr (Tantalo et al. 1996) or as late as ≳15 Gyr (Yi et al. 1998).

3. An established correlation seems to be in place between the PN luminosity-specific rate and $(B − V)$ color for elliptical galaxies in the Virgo and Fornax Clusters, and in the Leo group (Peimbert 1990; Hui et al. 1993). The sense is that the reddest metal-rich systems display, at the same time, a stronger UV upturn (Burstein et al. 1988) *and* a poorer PN population per unit galaxy luminosity (Buzzoni et al. 2006). If the PN event is the final fate for AGB stars at the end of their thermal pulsing phase (Iben & Renzini 1983), then the relative deficiency of nebulae might be evidence of an incomplete (or fully inhibited) AGB evolution of low-mass stars under special environment conditions of the parent galaxy.

As a central issue in this discussion, *it is clear therefore that a preeminent connection should exist between UV excess and AGB distinctive properties of stellar populations in early-type galaxies*.

According to the fuel consumption theorem (Renzini & Buzzoni 1986), a 1 $M_\odot$ star of solar metallicity enters its core He-burning phase with, at most, the equivalent of 0.43 $M_\odot$ of H to be spent as nuclear fuel.[3] This means that, under quite general conditions, post-RGB evolution alone could easily account, in principle, for up to $\frac{3}{4}$ of the total bolometric luminosity of a galaxy stellar population (Buzzoni 1998). Whether this energy is eventually reduced (if stars lose their fuel before they burn it), or whether it is finally released in the form of ultraviolet or infrared photons, crucially depends on mass loss and its impact along the entire red giant evolution. Hence, it is of special pertinence to constrain the relevant physical conditions that affect AGB evolution in favor of an earlier transition of HB stars toward high temperature and enhanced ultraviolet emission.

In this paper we would like to draw the reader's attention to a possibly new and powerful approach to the problem that can find straightforward applications even to distant galaxies. As explained in § 2, the method relies on surface brightness fluctuation theory to safely tie infrared effective magnitudes (that *can* be determined for unresolved stellar populations) to stellar luminosity at the AGB tip (that *cannot* be directly observed in distant galaxies). We show, in § 3, that these results tightly correlate with the ultraviolet properties of UV upturn elliptical galaxies, allowing a self-consistent physical picture and a quite accurate diagnostic of the post-RGB evolution of their underlying stellar populations, including HB morphology and AGB deployment. Our results are finally summarized and discussed in § 4.

2. INFRARED SURFACE BRIGHTNESS FLUCTUATIONS AS AGB PROBES

Tonry & Schneider (1988) and Tonry (1991) first realized the potentially useful information about the composing stars hidden in the surface brightness fluctuations (SBFs) of galaxies with unresolved stellar populations. The problem has since received a more complete theoretical assessment by Buzzoni (1989, 1993, 2008), Cerviño et al. (2000, 2002), and Cerviño & Luridiana (2006).

Briefly, the basic relationship on which the theory relies is

$$\frac{\sigma^2(L_{\mathrm{gal}})}{L_{\mathrm{gal}}} = \frac{\sum \ell_*^2}{\sum \ell_*} = \ell_{\mathrm{eff}}. \qquad (1)$$

The left-hand side of the equation links an observable quantity (namely, the relative variance of the galaxy surface brightness) with the theoretical second-order statistical moment of the composing stars. This quantity, in turn, traces the distribution of stellar luminosity (ℓ_*) for the whole population; it is also a natural output of any population synthesis code and can easily be computed for different photometric bands and distinctive evolutionary phases of simple stellar populations (SSPs; see, e.g., the current theoretical databases of Buzzoni 1993; Worthey 1993; Blakeslee et al. 2001; Cerviño et al. 2002; Cantiello et al. 2003; Raimondo et al. 2005; Mouhcine et al. 2005).

The derived "effective" stellar luminosity, ℓ_{eff}, in equation (1) has some important properties:

1. It can be derived from a fully observational procedure, without any supplementary theoretical assumptions.

2. It is an intrinsic distinctive parameter of the stellar aggregate, and its empirical measurement does not require any individual star to be (fully or partially) resolved.

3. It identifies an "effective" magnitude (i.e., $\overline{M} = −2.5 \log \ell_{\mathrm{eff}} + \mathrm{const}$) in a completely similar way and with the same photometric zero points as "standard" magnitudes, and it scales accordingly with distance and foreground screen reddening.

Being statistically representative of the stellar system as a whole, the effective magnitude cannot be physically associated to any specific star or stellar groups along the CMD of a stellar aggregate; nonetheless, it can be instructive to identify stars with $\overline{M}$ luminosity as the "prevailing" group tracing the whole population in the different photometric bands. This is shown in Figure 1 for the illustrative case of a 15 Gyr SSP with solar metallicity and Salpeter IMF. Because of the quadratic ℓ_* dependence of the summation in the numerator of equation (1), the effective magnitude at any optical/infrared band is highly sensitive to the giant stars and only marginally responds to a shift in the SSP "mass leverage" caused by a change in the IMF slope (Buzzoni 1993). Likewise, as probe of the brightest stars in a population at a given wavelength, the effective magnitude is relatively insensitive to any underlying older component in the case of composite stellar systems.[4]

It is evident from Figure 1 that near-infrared (near-IR) magnitudes closely trace the bright-end tail of the SSP luminosity function. In particular, one can notice that $\overline{K}$ is potentially the best tracer of the SSP tip stellar luminosity (K_{tip}), as *both quantities are expected to depend in quite the same way on the overall distinctive parameters of the stellar population, including age, metallicity, IMF, and mass loss*.[5] This is shown in Figure 2, where we compare the $\overline{K}$ versus K_{tip} relationship for a full collection of

---

[3] Under the most extreme hypothesis of no mass loss, a 1 $M_\odot$ star with solar abundance $(Y, Z) = (0.28, 0.02)$ starts its HB evolution with a total He amount of roughly 0.62 $M_\odot$, of which ~0.47 $M_\odot$ is confined in the core (Sweigart & Gross 1976) and $Y(1 − 0.47) \simeq 0.15 M_\odot$ reside in the envelope. Metals amount to roughly $Z(1 − 0.47) \simeq 0.01 M_\odot$ and, accordingly, fresh H is 0.37 $M_\odot$. Taking into account the nuclear rates (e.g., Cox & Giuli 1968), the H+He fuel provides at most the equivalent of $0.37 + 0.62/10 \simeq 0.43 M_\odot$ of hydrogen.

[4] This fact has been observationally confirmed through the comparison between SBF measurements in early-type galaxies and Magellanic star clusters (see González et al. 2004; González-Lopezlira et al. 2005).

[5] In spite of probing a relative minority of bright giant stars, the infrared effective magnitude is a fully robust characteristic parameter of a stellar population, in the case of galactic mass scales. From a statistical point of view, in fact, taking the reference SSP of Fig. 1 as representative of the elliptical galaxy stellar population, one has to expect about 9×10^7 "effective contributors" (in the statistical definition of Buzzoni 1993) to the K-band SBF for a galaxy of $10^{11} M_\odot$. This number further increases to about 10^8 for H-band contributors and to ~3 × 10^8 for the J-band SBF.
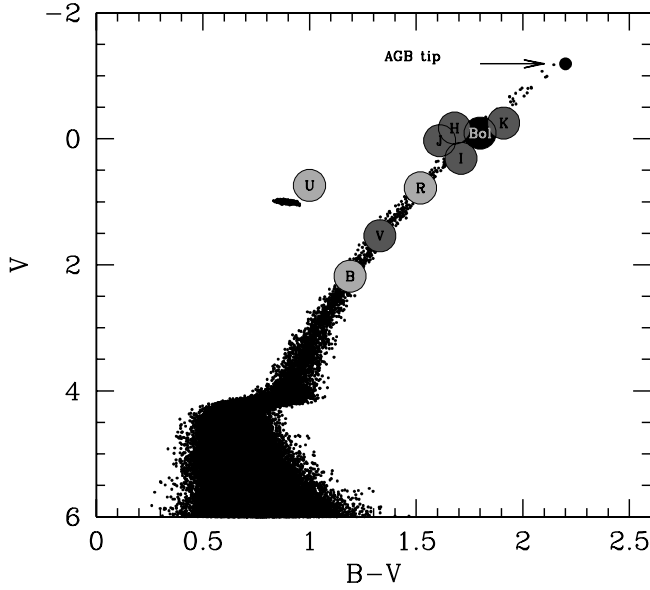
FIG. 1.—Illustrative V vs. $B - V$ synthetic CMD for a 15 Gyr SSP of solar metallicity and Salpeter IMF, with circles identifying the different effective contributors (i.e., the appropriate magnitude $M \equiv \overline{M}$) at various photometric bands (and to bolometric luminosity, as well). Although the different effective magnitudes cannot univocally be attributed to any $B - V$ color, one could let the prevailing stellar contributors to bolometric, infrared, and visual fluctuations arbitrarily coincide with the corresponding RGB location in the CMD. This is not the case for the U band, where the effective magnitude comes from a more entangled mix of HB, red giants, and bright MS stars about the turnoff region of the diagram. [*See the electronic edition of the Journal for a color version of this figure.*]

SSP models from the Buzzoni (1989) and the updated Charlot & Bruzual (CB07; Bruzual 2007) synthesis codes.[6,7]

The correlation appears quite robust, in spite of the extremely wide range explored for the population parameters and the different input physics adopted by the two sets of theoretical models.

Formal fits to the whole sets of models yield

$$K_{\mathrm{tip}} = \begin{cases} 0.75\overline{K} - 3.15 & \text{(Buzzoni 1989)}, \\ \quad \sigma = \pm 0.12 \text{ mag} \\ 0.74\overline{K}_s - 3.07 & \text{(Bruzual 2007)}. \\ \quad \sigma = \pm 0.25 \text{ mag} \end{cases} \quad (2)$$

2.1. AGB Completion in Young Stellar Populations: The Case of Magellanic Star Clusters

A comparison with real stellar populations extending across the widest range of evolutionary parameters would clearly be the ideal test for the envisaged theoretical picture. The Magellanic Clouds (MCs) stand out as striking candidates in this regard, with the age of their star clusters spanning over 4 orders of magnitude, from a few Myr up to $\sim 10^{10}$ yr. In addition, their relatively

---

[6] The K_s band is a variant of the standard K filter, sometimes preferred for its reduced background noise (see Persson et al. 1998 for specific details). Both filters have similar effective wavelength and photometric zero points, so that $K = K_s$ within a typical ± 0.03 mag uncertainty, as we directly verified in our tests.

[7] For the CB07 models, the fluctuation luminosity has been computed via eq. (1) from the original isochrone set, while K_{tip} is just read as the absolute magnitude of the brightest stellar type in the AGB+RGB phases.
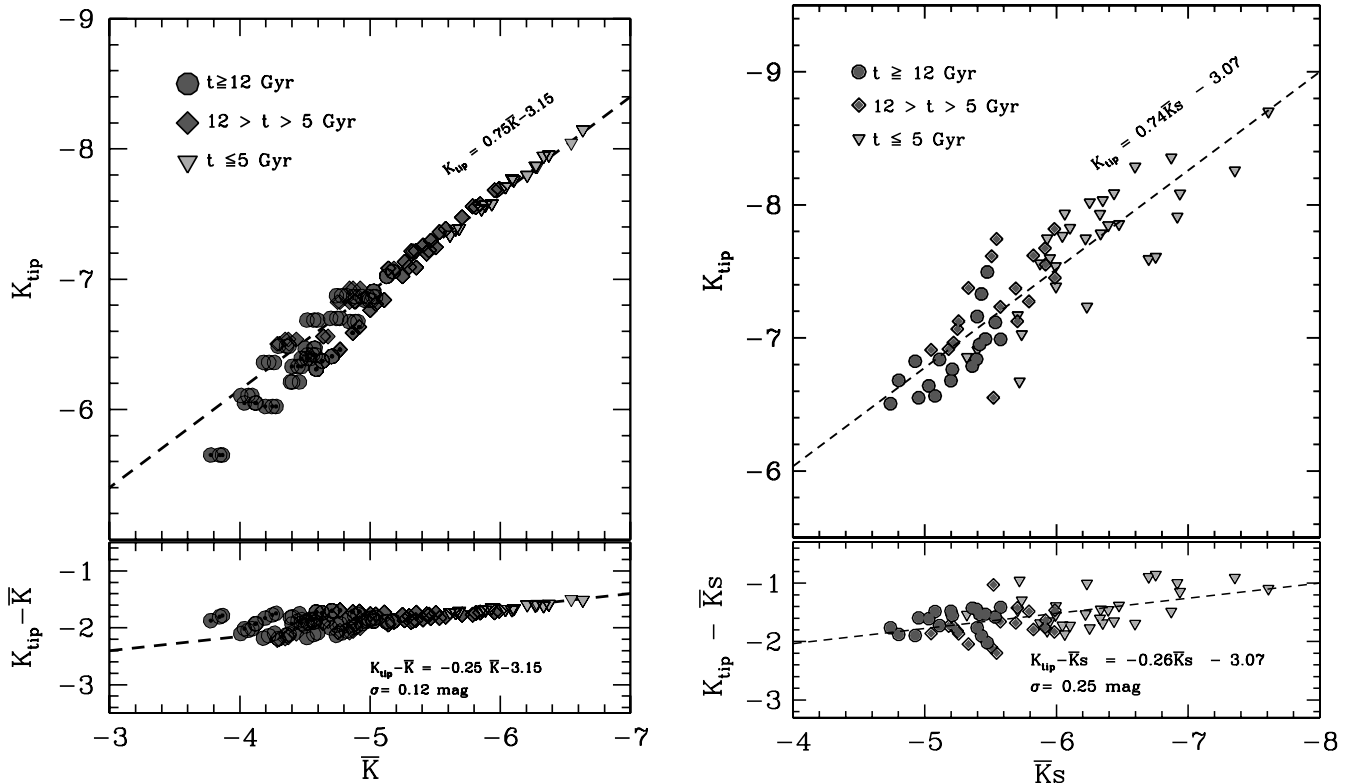

FIG. 2.— Theoretical relationship between near-IR effective magnitude and AGB+RGB tip luminosity for a full collection of SSP models from Buzzoni (1989, *left*) and CB07 (Bruzual 2007, *right*). Population ages span from 1 Gyr (*top right*) to 18 Gyr (*bottom left*); metallicity in the range $0.0001 \leq Z \leq 0.05$. The Buzzoni models explore a Reimers (1975) mass-loss parameter $\eta = 0.3$ and 0.5 for a Salpeter IMF, while the CB07 calculations adopt the mass-loss rates derived by Marigo & Girardi (2007) and use a Chabrier (2003) IMF. Dashed lines indicate fits to all points. Besides the overall agreement between the two synthesis codes, one has to notice a larger scatter around the mean relation for the CB07 models, mainly due to a different response to SSP metallicity at younger ages. [*See the electronic edition of the Journal for a color version of this figure.*]

TABLE 1
PARAMETERS OF MC STELLAR ''SUPERCLUSTERS''

SWB Type (1)	$\overline{M}_{K_s}$ (mag) (2)	$M_{K_{tip}}$ (mag) (3)	Log Age (yr) (4)	$\log Z$ (5)
Pre	-7.70 ± 0.40	-8.7 ± 0.2	6.4 ± 0.3	-0.3 ± 0.2
I	-8.85 ± 0.12	-9.8 ± 0.2	7.0 ± 0.3	-0.3 ± 0.2
II	-7.84 ± 0.28	-8.9 ± 0.2	7.5 ± 0.3	-0.3 ± 0.2
III	-7.45 ± 0.24	-8.3 ± 0.2	8.0 ± 0.3	-0.1 ± 0.2
IV	-7.51 ± 0.18	-8.4 ± 0.2	8.5 ± 0.3	-0.8 ± 0.2
V	-6.69 ± 0.20	-8.0 ± 0.2	9.0 ± 0.3	-0.6 ± 0.2
VI	-6.21 ± 0.24	-7.6 ± 0.2	9.5 ± 0.3	-1.0 ± 0.2
VII	-4.92 ± 0.38	-7.2 ± 0.2	9.9 ± 0.3	-1.4 ± 0.2

NOTES.—Col. (2): $\overline{M}_{K_s}$ from González et al. (2004, 2005). Col. (4): Ages from Frogel et al. (1990) corrected to the Large Magellanic Cloud distance modulus, $(m - M)_0 = 18.5$, as in Mouhcine et al. (2005). The age of the pre-SWB supercluster is also from González et al. (2004). Col. (5): Metallicities from Cohen (1982) for cluster types pre-SWB, I, and II, and from Frogel et al. (1990) for later types.

close distance allows *both* fluctuation luminosity *and* AGB/RGB luminosity tip to be directly measured on resolved CMDs.

Near-IR SBFs for a sample of 191 MC star clusters have been obtained by González et al. (2004, 2005) using K_s-band data from the Two Micron All Sky Survey (2MASS; Skrutskie et al. 1997). To reduce stochastic effects due to small-number stellar statistics along fast evolutionary phases, in their study these authors assembled seven "superclusters," by homogeneously co-adding several objects for each age class according to the Searle et al. (1980) SWB classification scheme.

The procedure to obtain the SBFs for these data has been extensively described before (González et al. 2004; Mouhcine et al. 2005); briefly, direct summation of bright stars provided the numerator of the right-hand fraction of equation (1), while total luminosity (at the denominator of the equation) was safely estimated from integrated photometry of each supercluster mosaic, to include the contribution of faint, unresolved stars. Following Lee et al. (1993) for the present work we have determined the tip luminosity of the AGB+RGB by convolving the luminosity function of each supercluster with a Sobel edge-detection filter (the zero-sum kernel [-2, 0, $+2$]). The tip luminosity was identified with the peak of the filter response function, after checking that there is indeed an important count discontinuity at that location in the luminosity function; the error in the measurement equals the width of the histogram bin. We list in Table 1 the K_s-band absolute fluctuation magnitude, K_s absolute tip magnitude, age, and metallicity of the MC superclusters.

Again, a tight relationship between K_{tip} and effective $\overline{K}$ magnitudes is in place, as shown in Figure 3, along the entire age range (and the corresponding metallicity drift; see Table 1, col. [5]). A fit to the MC data (Fig. 3, *dashed line*) provides

$$K_{tip} = 0.72\overline{K}_s - 3.26, \qquad (3)$$

with a data scatter $\sigma = \pm 0.21$ mag across the fitting line. Note that this perfectly compares, within the statistical uncertainty of the observations, with the equations in equation (2); this is true even beyond the nominal age range of the theoretical relations since, for instance, the pre-SWB and the SWB type I MC superclusters are too young to even sport any standard AGB or RGB phase.

2.2. Mass Loss and Post-RGB Evolution in Evolved Stellar Populations

The link between $\overline{K}$ and K_{tip} can be regarded as a *much more deeply intrinsic property of SSPs*, not exclusively related to age
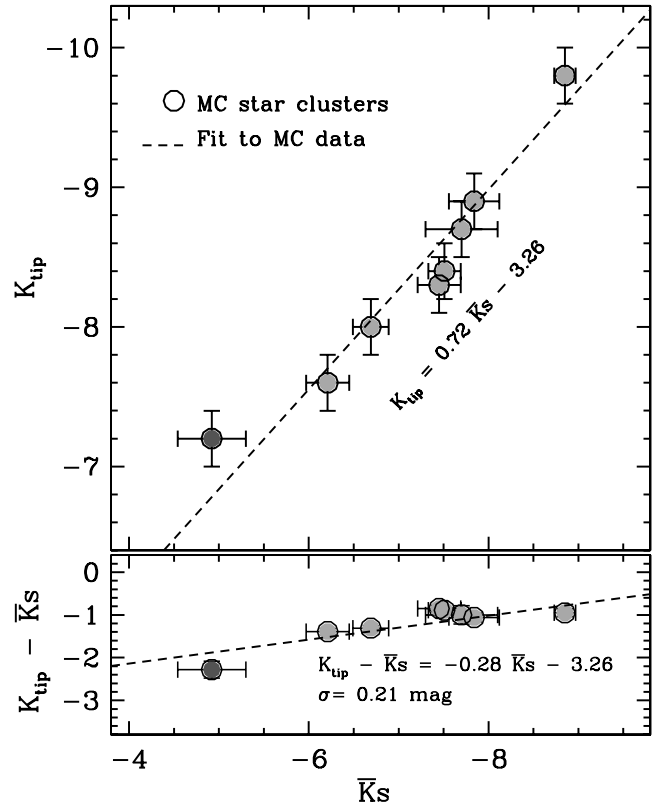

FIG. 3.—Absolute K_{tip} vs. $\overline{K}_s$ magnitude relationship for Magellanic Cloud star clusters. Circles locate the average position for each "supercluster" of Table 1, i.e., a co-addition of several individual systems belonging to homogenous Searle et al. (1980) age classes. The dashed line is the fit to the data, as displayed on the plot. Color code for markers is the same as in Fig. 2. [*See the electronic edition of the Journal for a color version of this figure.*]

(or metallicity) evolution. Of course, our method cannot remove, by itself, any age/metallicity degeneracy that makes integrated photometric properties of young metal-rich stellar systems closely resemble those of older metal-poor ones (e.g., Renzini & Buzzoni 1986; Worthey 1994). However, as far as old stellar populations are concerned, the unbiased and model-independent estimate of the tip stellar luminosity, even in unresolved stellar populations, provides an additional and powerful tool to quantitatively size up important effects, like the mass-loss impact on red giant evolution.

Relying on the Reimers (1975) standard η parameterization, Figure 4 gives an instructive example of how mass loss can modulate both K_{tip} and $\overline{K}$. In the figure we explore the behavior of an old (15 Gyr) SSP reference model (Fig. 4, *circles*), along a full variety of mass-loss scenarios, spanning from a virtually vanishing stellar wind (i.e., $\eta = 0$), up to a violent mass-loss rate ($\eta \rightarrow 1.5$) capable of fully wiping out the external envelope of stars while on the RGB phase. Similarly to Figure 3, we still report the same clean relationship between K_{tip} and $\overline{K}$, with old AGB-enhanced models ($\eta \rightarrow 0$) all closely resembling young (2–5 Gyr), standard ($\eta \simeq 0.3$) populations in the top right corner of the panel.

Again, according to the trend of the 15 Gyr model sequence versus η we can propose the following parametric equations:

$$K_{tip} \simeq 1.7\eta - 7.7,$$
$$\overline{K} \simeq 2.1\eta - 5.9. \qquad (4)$$

Curiously enough, note from the equation set that K_{tip} seems slightly less sensitive to η than does $\overline{K}$. As we see below, such a
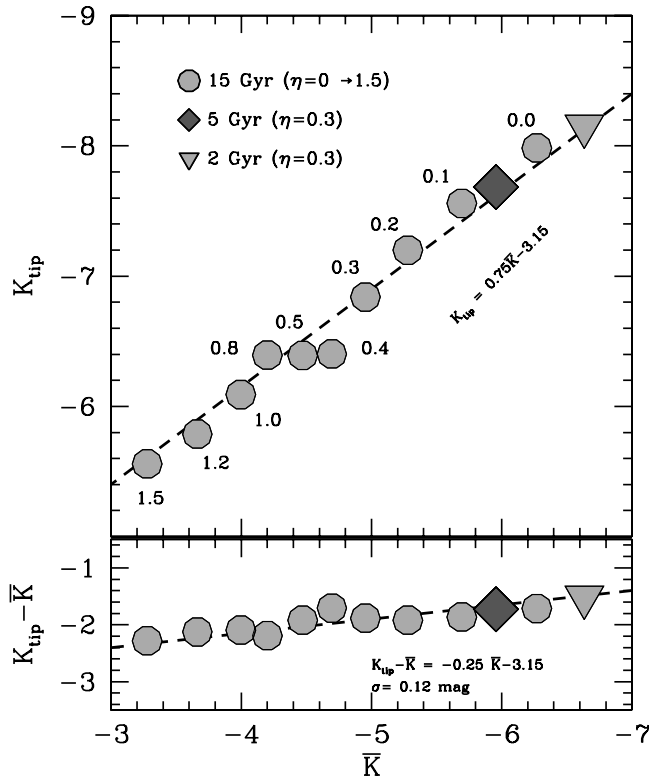
FIG. 4.—Theoretical relationship between K_{tip} and $\overline{K}$ with varying mass-loss efficiency along red giant evolution. Circles trace the change in a 15 Gyr old SSP of solar metallicity (Buzzoni 1989), with the increase of Reimers mass-loss parameter η from 0 to 1.5, as labeled on the plot. Note that a reduced mass loss ($\eta \rightarrow 0$) leads old SSPs to fully deploy the AGB and closely resemble much younger 2–5 Gyr old SSPs (*triangles and diamonds*) with $\eta = 0.3$ and otherwise similar distinctive parameters. [*See the electronic edition of the Journal for a color version of this figure.*]

FIG. 5.—Theoretical $\overline{K}$ and K_{tip} relationship with increasing mass-loss rate along red giant evolution. The illustrative case of a 15 Gyr old SSP of solar metallicity, after Buzzoni (1989) is considered. Note that for $\eta \lesssim 0.4$, the AGB luminosity tip is brighter than the RGB, and PNe are produced; if mass loss increases, then AGB luminosity is further reduced (and PN formation correspondingly thwarted), until stars at the RGB tip begin to dominate as the brightest objects in the population ($\eta \gtrsim 0.5$). For even higher mass-loss rates ($\eta \gtrsim 0.8$), stars undergo incomplete RGB evolution, leaving the branch "midway" and igniting helium at a higher effective temperature (hot flashers). [*See the electronic edition of the Journal for a color version of this figure.*]

smaller variation range for K_{tip} stems from the "bottoming out" effect of the RGB tip that eventually replaces the AGB in providing the brightest stars in a SSP when mass loss increases to $\eta \gg 0.5$.

The now established importance of mass loss in old stellar populations dominated by stars with $M_* \simeq 1\ M_\odot$ was first emphasized in a series of important theoretical contributions in the early seventies (Castellani & Renzini 1968; Iben & Rood 1970; Castellani et al. 1970); this was urged by the intervening observational evidence that a mass spread was needed to reproduce HB and AGB morphology in Galactic globular clusters (Demarque et al. 1972; Renzini 1977; Iben & Renzini 1983). To consistently match the observed AGB tip in local globular clusters, for instance, Fusi Pecci & Renzini (1976) suggested a fine-tuning value of $\eta \simeq 0.4 \pm 0.1$. This calibration for old Population II stars might not, however, be extended so straightforwardly, a priori, to more metal-rich environments, as one could realistically expect mass-loss efficiency to depend on (increase with?) metallicity.

Depending on mass-loss strength, standard stellar evolution theory basically features three characteristic scenarios that constrain post-RGB evolution of low-mass stars (see Fig. 5). Under different physical conditions and to a different extent, each one of these cases eventually leads to the formation of hot stars, thus potentially supplying an important contribution to the integrated ultraviolet luminosity of a galaxy:

1. For $\eta \lesssim 0.4$, models tell us that at the end of RGB evolution, low-mass stars ignite helium in a degenerate core (the so-called helium flash). A bright AGB evolution has to be expected, reaching
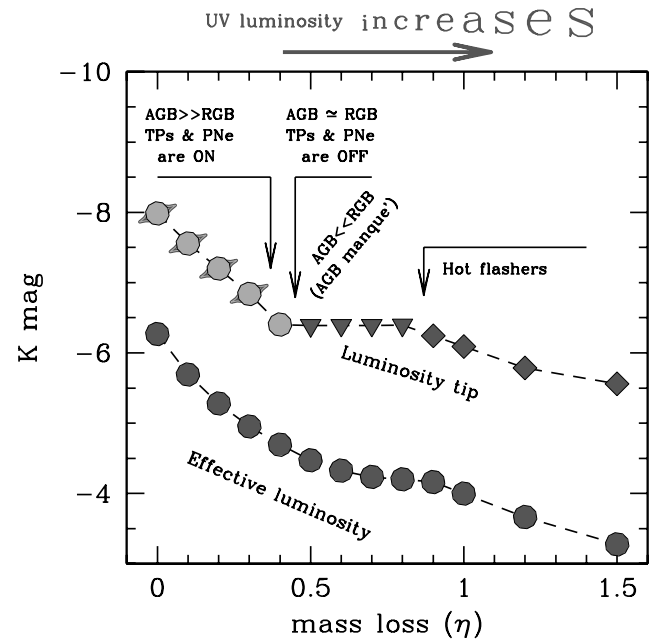
or even surpassing the RGB tip luminosity. If thermal pulses are set ($\eta \lesssim 0.3$), stars end up losing the external envelope and generating a planetary nebula (Iben & Renzini 1983). In this case, hot post-AGB nuclei of nebulae easily exceed an effective temperature of 30,000 K (Schönberner 1983).

2. If $\eta \gtrsim 0.4$, the PN event is aborted (Buzzoni et al. 2006), and AGB evolution is partially or fully inhibited (Greggio & Renzini 1990; Castellani & Tornambé 1991; Dorman et al. 1993). In this case, the brightest stars (in both bolometric luminosity and infrared) belong to the RGB tip, and they settle on the HB with a He core mass close or slightly exceeding 0.47 $M_\odot$ (e.g., Sweigart & Gross 1976; Seidel et al. 1987; Charbonnel et al. 1996; Piersanti et al. 2004). For slightly increasing mass-loss efficiency, the stellar envelope becomes thinner and thinner, and the hot internal core is unveiled. If this is the case, stars likely settle at high effective temperature ($T_{eff} \gg 20,000$ K) and originate a blue HB morphology.

3. As a final case, for an even stronger mass loss ($\eta \gtrsim 0.8$), the stellar envelope might be wiped out well before the full completion of the RGB phase. As a consequence, standard HB and AGB evolution would be fully inhibited; stars would be left "midway" along the RGB, with their rapidly exhausting H-shell emerging at ever shallower stellar layers. Such "hot flasher" stars would therefore postpone the He ignition by moving straight to the high-temperature region of the CMD, as is likely observed, indeed, in the cluster NGC 2808 (Sweigart et al. 2002; Castellani et al. 2006).

In terms of UV contribution, cases 1, 2, and 3 represent a sequence of increasing energy budget, since a prevailing fraction of stellar nuclear fuel is more efficiently burnt at high effective temperature. The outlined scenario has, of course, to be regarded as a general scheme, where the η thresholds discriminating

TABLE 2
SUMMARY OF RELEVANT DATA FOR THE ELLIPTICAL GALAXY SAMPLE

NGC (1)	$\log \sigma_v$ (km s^{-1}) (2)	Mg$_2 \pm \sigma$ (mag) (3)	$(B-V)_0$ (mag) (4)	$\log \alpha$ ($N_{PN}L_{gal}^{-1}$) (5)	$(1550-V)_0$ (mag) (6)	$\overline{F160W} \pm \sigma$ (mag) (7)	$\overline{K}_s \pm \sigma$ (mag) (8)	H$\beta \pm \sigma$ (Å) (9)
221....................	1.90 ± 0.03	0.198 ± 0.007	0.88	$-6.77^{0.18}_{0.31}$	4.50 ± 0.17	-5.28 ± 0.10	-5.95 ± 0.14	2.30 ± 0.05
224....................	2.27 ± 0.03	0.324 ± 0.007	0.95	$-6.94^{0.15}_{0.22}$	3.51 ± 0.17	-4.46 ± 0.09	-5.69 ± 0.14	1.66 ± 0.07
1316..................	2.38 ± 0.08	0.265 ± 0.023	0.87	$-7.50^{0.07}_{0.07}$	5.0 ± 0.2	-5.39 ± 0.19	...	2.20 ± 0.07
1379..................	2.11 ± 0.13	0.269 ± 0.006	0.88	...	3.01 ± 0.10	-5.11 ± 0.19	-5.75 ± 0.12	1.70 ± 0.09
1387..................	...	...	0.98	...	2.16 ± 0.05	-5.4 ± 0.8	-5.77 ± 0.10	...
1389..................	2.12 ± 0.06	0.236 ± 0.002	0.90	...	3.38 ± 0.09	-5.16 ± 0.20	-6.35 ± 0.13	...
1399..................	2.52 ± 0.03	0.357 ± 0.007	0.95	$-7.30^{0.07}_{0.07}$	2.05 ± 0.17	-4.55 ± 0.16	-5.28 ± 0.15	1.41 ± 0.08
1404..................	2.39 ± 0.03	0.344 ± 0.007	0.95	...	3.30 ± 0.17	-4.76 ± 0.21	-5.53 ± 0.10	1.58 ± 0.08
3379..................	2.33 ± 0.03	0.329 ± 0.007	0.94	$-6.77^{0.03}_{0.03}$	3.86 ± 0.17	-4.70 ± 0.14	-5.43 ± 0.17	1.46 ± 0.16
3384..................	2.20 ± 0.11	0.296 ± 0.014	0.91	$-6.42^{0.10}_{0.10}$	3.9 ± 0.2	-4.82 ± 0.22	...	2.05 ± 0.11
4278..................	2.45 ± 0.03	0.293 ± 0.007	0.90	...	2.88 ± 0.17	-4.49 ± 0.22	...	1.37 ± 0.03
4374..................	2.48 ± 0.03	0.323 ± 0.007	0.94	$-6.77^{0.10}_{0.10}$	3.55 ± 0.17	...	-5.71 ± 0.25	1.70 ± 0.04
4406..................	2.42 ± 0.03	0.330 ± 0.007	0.90	$-6.89^{0.10}_{0.10}$	3.72 ± 0.17	...	-5.74 ± 0.12	1.61 ± 0.16
4472..................	2.49 ± 0.03	0.331 ± 0.007	0.95	$-7.16^{0.10}_{0.10}$	3.42 ± 0.17	-4.64 ± 0.11	-5.64 ± 0.13	1.52 ± 0.14
4486..................	2.60 ± 0.03	0.303 ± 0.007	0.93	$-7.10^{0.1}_{0.10}$	2.04 ± 0.17	...	...	1.38 ± 0.04
4552..................	2.44 ± 0.03	0.346 ± 0.007	0.94	...	2.35 ± 0.17	...	-5.86 ± 0.13	1.65 ± 0.04
4621..................	2.41 ± 0.03	0.355 ± 0.007	0.92	...	3.19 ± 0.17	...	-5.59 ± 0.21	1.43 ± 0.11
4649..................	2.56 ± 0.03	0.360 ± 0.007	0.95	$-7.22^{0.1}_{0.10}$	2.24 ± 0.17	...	...	1.26 ± 0.04

NOTES.—Cols. (2, 3): The $\log \sigma$ and Mg$_2$ index from Burstein et al. (1988) except for NGC 1316, 1379, 1389, and 3384, which are averages from the Hyperleda database (Paturel et al. 2003). Col. (4): $(B-V)_0$ from the RC3 Catalog (de Vaucouleurs et al. 1991). Col. (5): The $\log \alpha$ from Buzzoni et al. (2006). Col. (6): $(1550-V)$ color from Burstein et al. (1988) except for NGC 1379, 1387, 1389, and 1404; these were scanned from Lee et al. (2005) with the Dexter package (Demleitner et al. 2001) and transformed according to the Colina et al. (1996) calibration scale. Col. (7): $\overline{M}_{F160W}$ from Jensen et al. (2003). Col. (8): $\overline{M}_{K_s}$ from Liu et al. (2002) (assuming the Cepheids distance modulus for the Fornax Cluster), excepting NGC 221, 224, 3379, and 4374, which are from Pahre & Mould (1994) and NGC 4406 and 4472, which are from Jensen et al. (1998). Col. (9): Hβ index from Jensen et al. (2003), except for NGC 4278, 4374, 4486, 4649, and 4552, estimated from Kobayashi & Arimoto (1999) and NGC 4621, derived from Kuntschner et al. (2001).

among the different evolutionary regimes slightly depend on SSP age (through the main-sequence turnoff [MSTO] mass). While the illustrative case of Figure 5 refers to a 15 Gyr SSP, one could easily verify that the overall trend for K luminosity is maintained, for instance, for a 10 Gyr population by just "shrinking" the η-scale of the plot by a factor of ~ 1.5 times; this means, for example, that AGB-manqué stars are produced in a 10 Gyr scenario for $\eta \gtrsim 0.6$.

3. UV UPTURN AND AGB DEPLOYMENT IN ELLIPTICAL GALAXIES

In order to assess the relevance of the previous theoretical framework to the appearance and strength of the UV upturn phenomenon in ellipticals, it is convenient to parameterize our analysis in terms of the $(1550-V)$ color, that is, a measure of the galaxy emission around the 1550 Å region versus the Johnson visual band, as originally defined by Burstein et al. (1988). To this end, the Burstein et al. (1988) *IUE* galaxy sample has been taken as a reference; we supply in Table 2, for each object, the infrared effective magnitudes from Jensen et al. (2003), Liu et al. (2002), Pahre & Mould (1994), and Jensen et al. (1998) and, when available, further relevant pieces of information, like stellar velocity dispersion, integrated $(B-V)$ color, Hβ and Mg$_2$ Lick indices, and the specific PN rate per unit galaxy luminosity (from Buzzoni et al. 2006).

As a first relevant clue in our analysis, Figure 6 suggests a trend among most ellipticals, with UV-enhanced galaxies being about 1 mag fainter in K_s effective magnitude (some 0.7 mag in the inferred K_{tip}) than UV-poor systems.[8] On the plot one should

note, however, a couple of outliers, displaying a brighter $\overline{K}$ magnitude [or, alternatively, a "bluer" $(1550-V)$ color]. These include NGC 1387 and NGC 1389 in the Fornax Cluster and NGC 4552 in Virgo. We will return to these objects in § 4 for a brief discussion. In addition, we have to mention that the "merger" radio-galaxy NGC 1316 (Fornax A) exhibits visible dust lanes that,
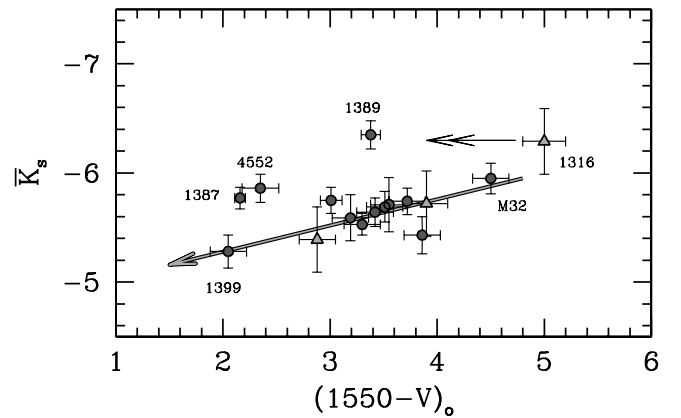

FIG. 6.— Absolute fluctuation magnitudes vs. ultraviolet color $(1550-V)$ for the galaxy sample of Table 2. Both $\overline{K}_s$ and $(1550-V)$ have been duly corrected for Galactic reddening. Triangles mark galaxies with $\overline{K}_s$ extrapolated from $\overline{F160W}$, as explained in footnote 6. Note the outlying cases of NGC 1387, NGC 4552, and NGC 1389 with an infrared effective magnitude that is ~ 0.7 mag too bright for their UV excess. The relevant case of the merger radio galaxy NGC 1316 (Fornax A) is also singled out in the plot, where the arrow indicates that a bluer $(1550-V)$ color might be more appropriate for this galaxy (with a more negligible impact on $\overline{K}_s$, however), as a consequence of a strong internal absorption due to the observed presence of dust lanes. Excluding these controversial objects (discussed in more detail in § 4), the data sample correlates fairly well ($\rho = -0.75$; see arrow), indicating a less deployed AGB for UV-enhanced galaxies. [*See the electronic edition of the Journal for a color version of this figure.*]
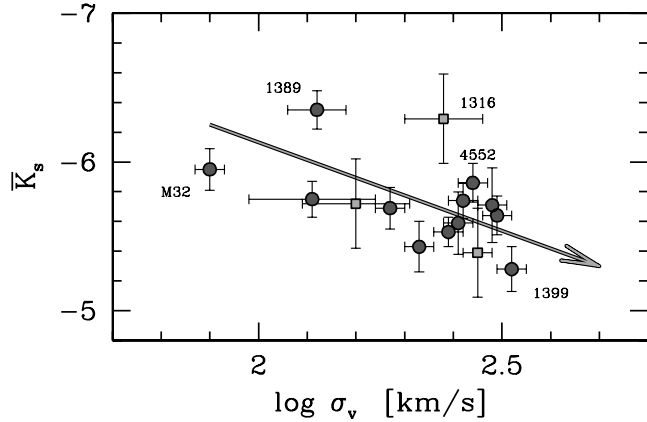
[8] In order to increase the displayed galaxy sample on the different plots that involve infrared photometry, for some objects we derived the K-band effective luminosities based on the F160W $\equiv H$ photometry only assuming, empirically from Table 2, $\langle \overline{H} - \overline{K}_s \rangle = +0.9$, with a conservative error bar of ± 0.3 mag. The extrapolated $\overline{K}$-mag data are displayed with a different marker on the plots.

Fig. 7.—Absolute fluctuation magnitudes vs. velocity dispersion for the galaxy sample of Table 2. Squares mark galaxies with $\overline{K}_s$ extrapolated from $\overline{F160W}$, as explained in footnote 6. [*See the electronic edition of the Journal for a color version of this figure.*]

Fig. 8.—Luminosity-specific PN number (α) vs. effective K luminosity for the galaxy sample of Table 2. The triangles mark galaxies with $\overline{K}_s$ inferred from $\overline{F160W}$ (see footnote 6). Note that a fainter AGB roughly correlates with a scantier PN stellar population among old/metal-rich (UV-enhanced) ellipticals, as expected from the long post-AGB to PN nucleus transition time, combined with the (shorter) evaporation timescale of the ejecta (compare the sketch on the plot with Fig. 15 of Buzzoni et al. 2006). A correspondingly low PN rate per unit galaxy luminosity is also to be expected, on the other hand, for younger stellar populations, as in the case of NGC 1316, as a consequence of higher stellar masses and a reduced PN nuclear lifetime. [*See the electronic edition of the Journal for a color version of this figure.*]

when accounted for, may lead to an intrinsically bluer (1550-V) color, although with possibly negligible effects on the K SBF magnitude.

After excluding these controversial objects, the data tend to display a fairly good correlation ($\rho = -0.75$) that, also recalling equation (4), we can approximate with

$$\Delta \overline{K}_s \simeq 1.4 \Delta K_{\text{tip}} \simeq -0.2 \Delta (1550 - V). \qquad (5)$$

If we entirely ascribe the dimming in red giant tip luminosity suggested by Figure 6 to a mass-loss effect, then equation (4) implies a spread $\Delta \eta \simeq 0.4$ among the galaxy population, with UV-enhanced ellipticals requiring a Reimers parameter $\eta \simeq 0.3$–0.4, very similar to what Fusi Pecci & Renzini (1976) derived empirically for the Galactic globular clusters. According to Figure 5, this confirms that, overall, the AGB is deployed in luminosity slightly above the RGB tip, so that the brightest stars in ellipticals should indeed always be genuine AGB stars.

There is an obvious caveat, however, in this simplified picture. If a standard monolithic scenario is assumed for early-type galaxy formation, then gravitational collapse of the primeval gas clouds should have proceeded over a free-fall timescale $\tau_{\text{ff}} \propto \sigma_v^{-1} \propto M_{\text{gal}}^{-1/2}$ (e.g., Larson 1974), leading to a mass-age-metallicity relation for early-type galaxies, where more massive galaxies are both older and more metal-rich than less massive ones (e.g., Pahre et al. 1998). The combined action of age and metallicity plays an important role to modulate the red giant luminosity tip, as the AGB is "naturally" brighter among young or metal-rich SSPs (see, again, Fig. 3).

The complex interplay of the different galaxy physical properties is well depicted in Figures 7 and 8. For one, as Burstein et al. (1988) had already shown, the UV upturn seems to appear among the most massive and metal-rich ellipticals (i.e., there is a positive correlation with σ_v and the Mg$_2$ index, respectively). Figure 7 also indicates for these galaxies a less extended AGB, as for a lower stellar core-mass distribution. This feature is likewise expected to directly affect the PN rate per unit galaxy luminosity (the so-called α index; see Fig. 8); indeed, there is a scantier PN stellar population among old/metal-rich (UV-enhanced) ellipticals (Ferguson & Davidsen 1993; Buzzoni et al. 2006).

3.1. Constraints on HB Morphology

Observations of local star samples show that the Hβ index reaches its maximum strength for A-type stars in the temperature
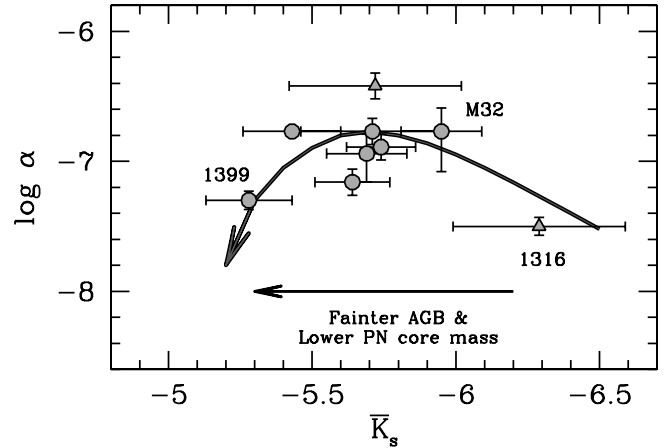
range $T_{\text{eff}} \simeq 8000 \to 10,000$ K (Buzzoni et al. 1994). Given this selected sensitivity, synthesis models of old SSPs (Buzzoni et al. 1994; Maraston et al. 2001) predict the integrated index to be strongly enhanced (by roughly 0.8 Å or more) in the presence of a broad color-extended HB, as observed for most metal-poor Galactic globular clusters. This important piece of information could therefore usefully complement the more extreme (1550 − V) color in the analysis of HB morphology for unresolved stellar populations in distant galaxies.

The situation is summarized in Figure 9, where elliptical galaxy data are compared with three illustrative cases of 15 Gyr SSPs with slightly supersolar metallicity ([Fe/H] = +0.3) and different ranges of HB temperature distribution. In particular, in the
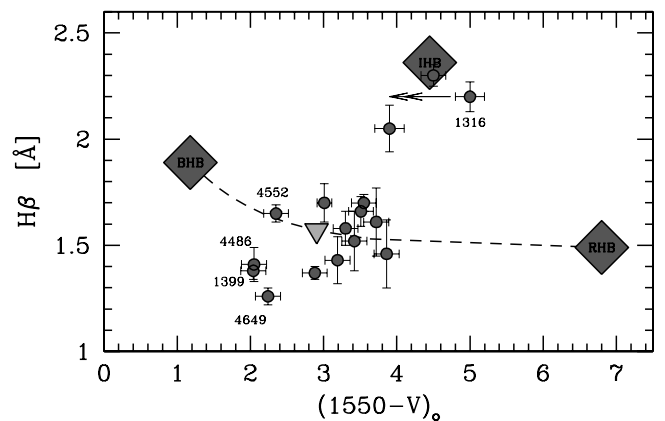

Fig. 9.—Lick Hβ index vs. (reddening-corrected) UV color $(1550 − V)_0$, for the galaxy sample in Table 2. Three reference SSP models are superposed, after Buzzoni (1989) exploring different HB morphologies (namely, RHB, IHB, and BHB temperature distributions, as explained in the text), assuming a 15 Gyr, slightly metal-rich ([Fe/H] = +0.2), with a fixed Reimers mass-loss parameter ($\eta = 0.3$) stellar population. Note that the bulk of UV upturn ellipticals need a mixture of blue and red HB stars, roughly in proportion of [N(RHB):N(BHB)] = [80:20], as marked by the triangle in the plot. For this composite stellar population, Fig. 10 reports the resulting synthetic CMD and the integrated SED. [*See the electronic edition of the Journal for a color version of this figure.*]
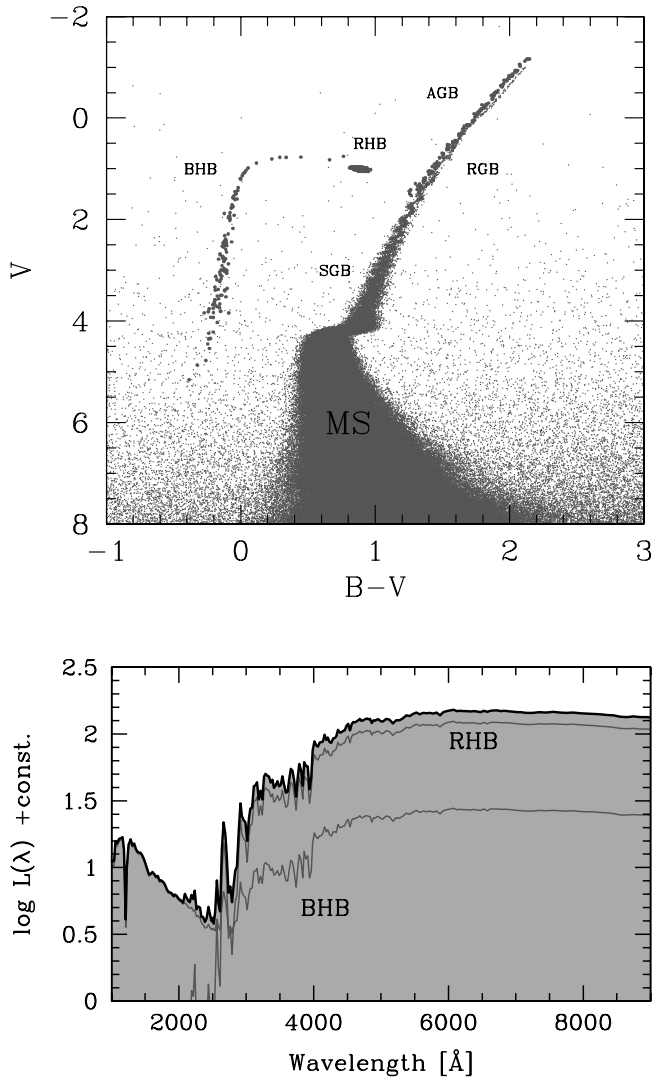
Fig. 10.—*Left*: Synthetic CMD for the reference composite stellar population matching UV upturn ellipticals, as discussed in Fig. 9 (the corresponding triangle in the plot), after Buzzoni (1989). The resulting mix assumes a bimodal HB morphology, with a prevailing bulk of RHB stars and a hot tail (BHB), extending up to $T_{\rm eff} \simeq 40{,}000$ K. The RHB stellar component provides about 80% of the total luminosity. An age of 15 Gyr is assumed in all cases, with a moderately metal-rich chemical composition (i.e., [Fe/H] = +0.2), a Salpeter IMF, and a fixed Reimers mass-loss parameter $\eta = 0.3$. A Poissonian error is artificially added to the data to better appreciate the number density distribution of stars along the different evolutionary branches of the diagram. The integrated SED of the whole population is displayed in the right panel, disaggregating the luminosity contribution from the two star samples. [*See the electronic edition of the Journal for a color version of this figure.*]

figure we account for (1) a red HB (RHB) morphology, that is, a clump of red stars very close to the RGB location, mimicking the real case of metal-rich Galactic globular clusters, like 47 Tuc; (2) an intermediate HB (IHB) morphology, with a broad (roughly bell-shaped) temperature distribution peaked about the A-stars' temperature range and extending up to $T_{\rm eff} \sim 12{,}000$ K; (3) a blue HB (BHB) morphology, peaked at 20,000 K and with a tail of hot sdB stars, up to a temperature of 40,000 K (see Buzzoni 1989 for further details).

Interestingly enough, the comparison with the observations shows that UV upturn ellipticals *cannot* be compatible with any BHB morphology alone. Too many hot stars would make the 1550 Å galaxy luminosity exceedingly bright compared to the energy bulk released at the *V* band. On the other hand, neither an
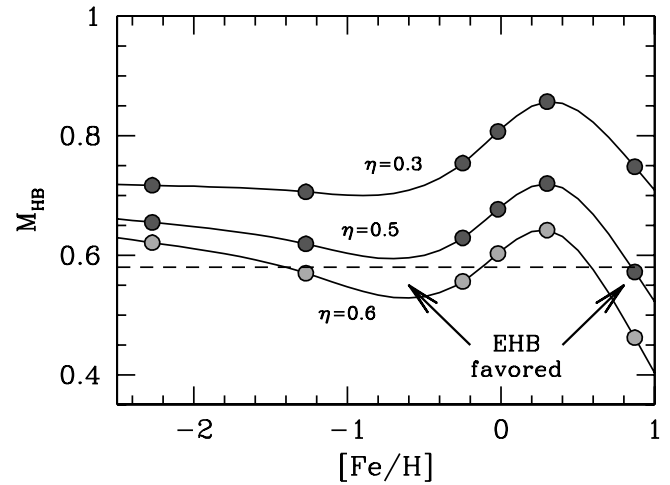

Fig. 11.—Expected representative stellar mass at the onset of the HB evolution for the Buzzoni (1989) 15 Gyr SSP models with different metallicity and mass-loss rate, according to a Reimers parameterization (η). In combination with a moderately enhanced ($\eta \simeq 0.5$ or higher) mass loss, two preferred ranges of metallicity (namely, [Fe/H] $\simeq -0.7$ and $\gtrsim + 0.5$ dex) may more easily favor the presence of low HB masses ($M_{\rm HB} \lesssim 0.58$ $M_\odot$; *see dashed line*) and the corresponding appearance of a hot-temperature tail in the HB morphology. [*See the electronic edition of the Journal for a color version of this figure.*]

IHB is viable, given the catastrophic impact of its A-star component on the integrated Hβ index of the population (e.g., Rose & Deng 1999). Definitely, an optimum match to these systems requires a mixed contribution, where the bulk of the galaxy luminosity (over 80%) is provided by standard (metal-rich) stellar populations with a red HB, on which a 20% (or less, in terms of total optical contribution) BHB component is superposed. Figure 10 provides an illustrative picture of this case, showing the synthetic CMD and the integrated SED for the composite stellar population corresponding to the big triangle in Figure 9.

So, in full agreement with the conclusions of Brown (2004), a somewhat dichotomous scenario seems to emerge for giant ellipticals, where the occurrence of the UV upturn phenomenon is intimately related to the appearance, among the galaxy HB population, of a hot and very low mass stellar component ($M_* \ll 0.58$ $M_\odot$; e.g., Sweigart & Gross 1976) that at some stage begins to join the standard red clump stars. It could be useful to note, in this regard, that two metallicity ranges seem to favor the formation of EHB stars through an optimum combination of MSTO stellar masses and subsequent mass loss via stellar winds along the RGB. As displayed in Figure 11, [Fe/H] values of either $\simeq -0.7$ or $\gtrsim +0.5$ dex provide, in principle, the needed low mass at the onset of HB evolution in a standard Reimers mass-loss framework with $\eta \gtrsim 0.5$.

To add even further to this challenging situation, however, one also has to report that high-resolution UV spectroscopy of a sample of six UV-strong ellipticals (namely, NGC 1399, 3115, 3379, 4472, 4552, and 4649) indicates for the claimed BHB component a moderately subsolar ($Z \sim 0.1$ $Z_\odot$) metallicity (Brown et al. 1997). If confirmed,[9] this result might lead to the identification of the *metal-poor* stellar component of giant ellipticals as the one responsible for the UV excess. Whatever the exact mechanism, this will cause HB morphology to readily assume a bimodal distribution, with a relative lack of warm stars at the intermediate $T_{\rm eff}$ range pertinent to the A spectral type (see Fig. 10).

---

[9] Surface metal abundance can easily be biased by diffusion mechanisms in the atmosphere of sdB stars (Unglaub & Bues 2001).

4. SUMMARY AND CONCLUSIONS

In this paper we have carried out a synoptic analysis of the different observational features that have to do with the UV luminosity excess in elliptical galaxies. As far as the canonical picture is assumed, with old stellar populations dominating early-type galaxy luminosity, the appearence of the UV upturn should readily call for a profound change in the CMD of galaxy stellar populations, not only involving the hot stellar component of the galaxy but also reverberating on red giant evolution at the low-temperature regime. As we mainly deal with distant, unresolved stellar populations, our analysis has to rely on a combined approach, matching infrared and ultraviolet diagnostic tools in order to probe the main features of the stellar CMD, starting with integrated galaxy photometry.

Theory of surface brightness fluctuations provides, in this sense, a natural and quite powerful way to go deep inside the problem and, as far as the infrared wavelength interval is considered, we have demonstrated theoretically that a straight and very clean relationship is in place between a macroscopic measure, such as the galaxy fluctuation magnitude and the corresponding individual magnitude of the brightest stars in turn at the tip of the red giant (AGB+RGB) phases (Fig. 2).

Played in the K band, this correlation leads, from a measurement of $\overline{K}$, to a value for $K_{\rm tip}$:

$$K_{\rm tip} = 0.75\overline{K} - 3.1, \qquad (6)$$

with a ± 0.2 mag internal uncertainty. As we showed in § 2, our SSP theoretical predictions find full support from the observations, and a direct check on the MC star clusters confirms the $\overline{K}$ versus $K_{\rm tip}$ relationship to be a much more general and deeply intrinsic property of stellar populations, virtually independent from any assumption about age, metallicity, IMF, and mass-loss parameters. Given its nature, this relationship cannot, by itself, help disentangle the problem of age/metallicity degeneracy; however, quite fruitfully, it provides us with a very direct probe of AGB properties, in a number of relevant details that directly deal with the mass-loss impact and the mass of dying stars (Fig. 4).

Our effort toward exploring the infrared side of galaxy SEDs has a twofold aim since, as a consequence of the basic principle of energy conservation, any gram of stellar fuel spent to feed ultraviolet luminosity cannot (and will not) be spent at longer wavelengths. This has led to the key issue of this paper, summarized in Figure 6, that the *strengthening of the UV rising branch is always seen to correspond to a weakening in the AGB luminosity extension*, as traced by galaxy K fluctuation magnitude.

This "shortening" in AGB deployment is mainly recognized among giant ellipticals ($\overline{K}$ becomes fainter with increasing galaxy velocity dispersion, σ_v; see Fig. 7) and could mainly be ascribed to an age effect, as the AGB tip naturally fades in luminosity with increasing age of the system (Fig. 3), and high-mass galaxies are recognized to be older than systems of lower mass (e.g., Burstein et al. 1988; Bressan et al. 1996; Liu et al. 2002; Jensen et al. 2003; González-Lópezlira et al. 2005; Renzini 2006). However, the relationship in place likely calls for a more elaborate physical scenario, once the full range of observing evidences is added to our analysis.

1. Besides being old, UV upturn galaxies are also metal-rich (i.e., stronger in Mg_2 Lick index). Disregarding any change in mass-loss rate, stellar tracks predict slightly more massive stars to evolve off the MS at a fixed age, with increasing metallicity
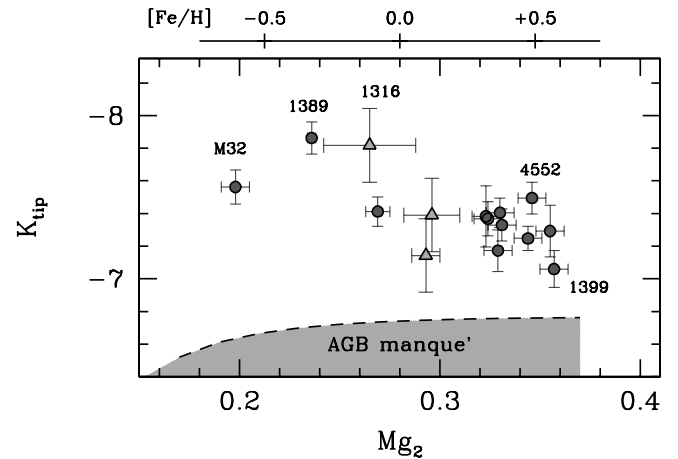

Fig. 12.—$K_{\rm tip}$ vs. Lick Mg_2 index for the galaxy sample in Table 2. The Lick index is assumed to trace galaxy metallicity according to the Buzzoni et al. (1992) calibration, as reported on the top axis of the plot. The observed decrease in $K_{\rm tip}$ with increasing [Fe/H] can be mostly explained if more metal-rich galaxies are also older, as in a standard monolithic scenario for galaxy formation. The dashed line marks the minimum luminosity required for stars to experience the thermal pulsing phase along their AGB evolution and thus end their evolution as PNe. [*See the electronic edition of the Journal for a color version of this figure.*]

(e.g., Bressan et al. 1994; Cantiello et al. 2003). This leads to correspondingly more massive AGB stars and a brighter AGB luminosity. Facing the observed trend in galaxy distribution, as summarized in Figure 12, metallicity effects evidently enter by mitigating the dimming action of age on $K_{\rm tip}$ with increasing galaxy mass. In any case, the interplay between age and metal abundance actually makes the derived range for the Reimers mass-loss parameter (i.e., $\Delta\eta \simeq 0.4$, as discussed in § 3) a safe upper limit. In fact, it suggests that metal abundance does *not* modulate by orders of magnitude mass-loss efficiency via stellar winds.[10]

2. A match of galaxy $\overline{K}$ data with the calibration of Figure 5 confirms that brightest stars in ellipticals are all genuine AGB members, reaching the thermal-pulsing phase (see also Fig. 12), with the AGB tip exceeding the RGB tip by some 0.5–1.5 mag. In the temperature range of M giant stars, a major fraction of bolometric luminosity is emitted through the K band and bolometric correction is a nearly constant quantity that we can estimate from $({\rm Bol} - K) = +2.75 \pm 0.2$ mag (Johnson 1966). We can therefore straightforwardly translate the galaxy fluctuation magnitude into an estimate of the bolometric tip luminosity, $L_*^{\rm tip}$, and from that the corresponding stellar core mass.[11] From our previous calibration (eq. [6]), we can then write

$$\log L_*^{\rm tip} = -0.4[(0.75\overline{K} - 3.1) + 2.75 - 4.72] \qquad (7)$$

---

[10] Observational evidence about the link between metallicity and mass loss in the Milky Way and the Magellanic Clouds is contradictory. For example, Groenewegen et al. (1995) find indications that mass-loss rate (not necessarily mass-loss *efficiency*) in single AGB stars is linearly proportional to Z. Conversely, also from data of single stars, van Loon (2000) argues that $\dot{M}$ is metallicity-independent. From a theoretical point of view, Cantiello et al. (2003) models suggest that, if mass loss is really proportional to metallicity, its effect to dim near-IR effective luminosities on average almost exactly offsets the brightening effect of metallicity itself.

[11] A somewhat linear relationship between stellar luminosity and core mass is a general consequence of any evolutionary stage characterized by a (multi) shell-burning regime in the presence of a relatively thin external envelope (Paczyński 1970). This is actually the case for both pre-He flash evolution along the RGB and the thermal pulsing phase along the AGB (see Iben & Renzini 1983 and Boothroyd & Sackmann 1988 for a more general discussion).
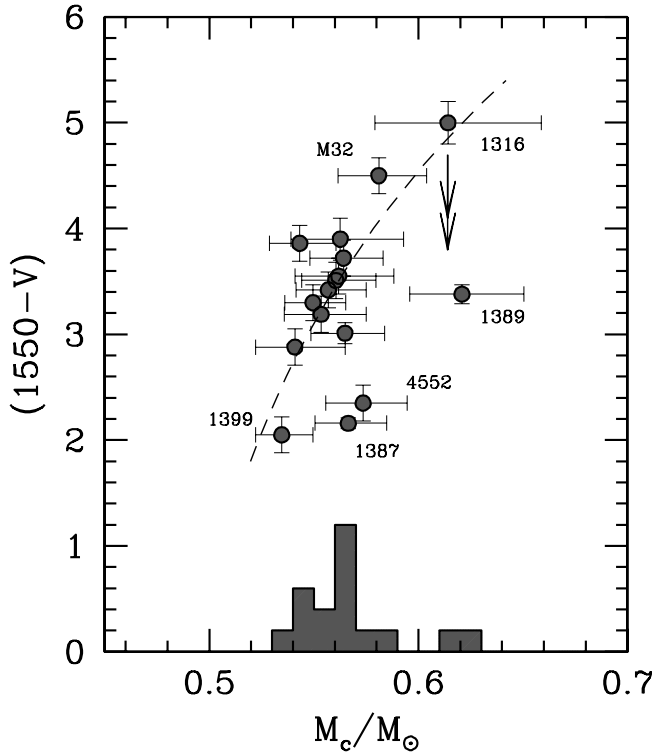
Fig. 13.—Observed ultraviolet color $(1550 - V)$ vs. core mass of stars at the AGB luminosity tip, as inferred from eq. (8), for the elliptical galaxy sample of Table 2. The M_c distribution is summarized in the lower histogram and is the maximum actual mass allowed to luminous stars in the galaxies. One sees that mass of dying stars tends to decrease with increasing UV upturn strength, being in general $\lesssim 0.57\ M_\odot$ among giant ellipticals. The "outlier" objects of Fig. 6 are identified again here, with galaxies labeled according to their NGC number. The arrow for NGC 1316 accounts for the claimed strong internal reddening for this galaxy. Displayed uncertainties for the derived values of M_c take in the full error budget—each component of $\sigma(M_c)$ being added in quadrature—including the contribution of $\overline{K}$ observations, K-band bolometric correction ($\sigma = \pm 0.2$ mag), and the $K_{\rm tip}$ vs. $\overline{K}$ calibration ($\sigma = \pm 0.2$ mag). See text for a discussion. [*See the electronic edition of the Journal for a color version of this figure.*]

(where the Sun has magnitude $M_{\rm Bol,\odot} = +4.72$). Following Boothroyd & Sackmann (1988) from the assumed core mass-luminosity relation for the solar metallicity range, this leads to

$$M_c = \frac{L_*^{\rm tip}}{52,000} + 0.456\ M_\odot. \qquad (8)$$

Figure 13 reports the inferred core-mass distribution, at the PN onset, for our galaxy sample.

Note that this is the *maximum* actual mass allowed to luminous stars in each galaxy environment and demonstrates that the *mass of dying stars tends to decrease with increasing UV upturn strength*, being in general $M_{\rm dying} \lesssim 0.57\ M_\odot$ among giant ellipticals. For this mass range, PN lifetime is the largest possible, but the time-scale for the nebula to be visible is critically constrained by the transition time ($\tau_{\rm tt}$) needed by the post-AGB stellar core to be hot enough to fire up the ejected envelope and become a hard UV emitter (Stanghellini & Renzini 2000; Marigo et al. 2004). The evident drop of α among strong UV upturn galaxies (Fig. 8) might be a direct consequence, therefore, of an increasing blocking effect of $\tau_{\rm tt}$ along the inferred M_c range (i.e., the stellar core takes longer to heat up than the shell to evaporate; Buzzoni et al. 2006), to which one has to further add a size cut in the overall PN population, as a result of the EHB progenitors ($M_* \lesssim 0.52\ M_\odot$) evolving as AGB-manqué stars and therefore skipping the nebula event.

3. We noted, in § 3, the importance of the integrated Hβ index as a fairly selective tracer of the warm ($T_{\rm eff} \simeq 8000$–10,000 K) stellar component in the galaxy stellar population. A proper assessment of the photometric contribution from this range of temperatures is of paramount importance in the framework of early-type galaxy evolution, in order to single out any signature of recent (i.e., in the last few Gyr or so) star formation or, conversely, of intervening evolution of the HB morphology among old SSPs, as in a more standard canonical scenario.

As far as UV upturn galaxies are concerned, the study of Hβ distribution clearly points to *a substantial lack of A-type stars* in the galaxy mix (see Fig. 9). While, on one hand, this definitely secures the "quiescent" nature of these galaxies, it also poses, on the other hand, a stringent constraint on HB morphology in their old-age context. In fact, a bimodal temperature distribution is required for the HB to assure, at one time, both an enhanced UV emission *and* a conveniently low Hβ feature. Thus, in these systems the expected prevailing bulk of red HB stars should be accompanied, at some point, by a residual population of blue (metal-poor?) HB objects (coincident with EHB stars in the current empirical classification scheme), peaked at $\sim$20,000–40,000 K, in a proportion of roughly $N_{\rm RHB} : N_{\rm BHB} \simeq [80:20]$.

On the other hand, to complete the picture, one cannot neglect the masking effects of age distribution, facing recognized evidence for low-mass ellipticals to display a more silent but also more continuous star formation along their entire galaxy life that naturally feeds the A-star contribution, thanks to the bluer MSTO point exhibited by SSPs in the $1-3$ Gyr age range, and leads to a younger "average" age, compared to high-mass systems. This is what we observe, for instance, among the resolved stellar populations of the Local Group dwarf spheroidals (Mateo 1998; see, in this regard, the illustrative location of M32 in Figure 9, and also consider the discussion by Schiavon et al. 2004).

4. Along with our discussion of the $\overline{K}$ versus $(1550 - V)$ relation, we noted in Figure 6 the presence of a few outliers about 0.7 mag brighter at infrared magnitudes or, alternatively, $\sim$1.5 mag bluer in the $(1550 - V)$ color, than the main galaxy population. In order to further investigate this issue, we tracked the relevant objects also in other figures whenever possible.

If galaxy mass (*alias* log σ_v) is considered as the leading physical parameter to compare outlier location with respect to the bulk of the galaxy distribution (see, e.g., Fig. 7), one must conclude that both NGC 4552 and NGC 1389 seem to have a brighter AGB tip rather than a bluer $(1550 - V)$ color. With regard to NGC 1389, Liu et al. (2002) find that the $\overline{K_s}$ SBFs of NGC 1389 are also too bright compared to its $(V - I)$ color, a fact that would be consistent with either a higher than average metallicity, given the age of its most recent burst of star formation, or a longer lifetime of its TP-AGB stars (Mouhcine et al. 2005). In the case of NGC 4552, however, Jensen et al. (1996) contribute an interesting piece of information. These authors measure near-IR SBFs for several galaxies in Virgo, and their results are systematically fainter than those obtained by Pahre & Mould (1994). Unfortunately, the two groups use slightly different filters (Jensen et al. employ K', vs. K_s of Pahre & Mold), but the discrepancy is larger than can be ascribed to the effect of the filters.[12] In particular, Jensen et al. find $\overline{K'} = -5.51$ for NGC 4552; assuming $\overline{K'} \equiv \overline{K_s}$, NGC 4552 would no longer be deviant in the $\overline{K_s}$ versus $(1500 - V)$ plane. Concerning NGC 1387, the dearth of data for this galaxy in the literature (see Table 2) makes it hard to propose an origin for its

---

[12] Jensen et al. (1996) attribute the difference to the higher S/N of their data; the S/N of the Liu et al. (2002) images is similar to that of Jensen et al.'s.

departure from the $\overline{K}_s$ versus $(1500 - V)$ sequence.[13] On the other hand, NGC 1387 and NGC 1389 are lenticular galaxies, like the merger remnant NGC 1316, but so are NGC 3384 and NGC 4406, both of which do not deviate from the correlation.[14]

---

[13] Note that NGC 1387 complies with the $\overline{K}_s$ vs. $(V - I)$ correlation determined by Liu et al. (2002).

[14] The other galaxies in our sample are all genuine ellipticals (de Vaucouleurs et al. 1991), except for NGC 224 (alias M31), which is so close, however, that bulge SBFs can be measured without any significant contamination from the disk.

At any rate, NGC 1387 and NGC 1389 constitute privileged candidates for any future "in-depth" investigation.

REFERENCES

Bailyn, C. D. 1995, ARA&A, 33, 133
Blakeslee, J. P., Vazdekis, A., & Ajhar, E. A. 2001, MNRAS, 320, 193
Boothroyd, A. I., & Sackmann, I.-J. 1988, ApJ, 328, 641
Bressan, A., Chiosi, C., & Fagotto, F. 1994, ApJS, 94, 63
Bressan, A., Chiosi, C., & Tantalo, R. 1996, A&A, 311, 425
Brown, D., Yi, S., Han, Z., & Yoon, S.-J. 2006, Baltic Astron., 15, 13
Brown, T. M. 2004, Ap&SS, 291, 215
Brown, T. M., Bowers, C. W., Kimble, R. A., Sweigart, A. V., & Ferguson, H. C. 2000, ApJ, 532, 308
Brown, T. M., Ferguson, H. C., Davidsen, A. F., & Dorman, B. 1997, ApJ, 482, 685
Brown, T. M., Ferguson, H. C., Smith, E., Bowers, C. W., Kimble, R. A., Renzini, A., & Rich, R. M. 2003, ApJ, 584, L69
Brown, T. M., Ferguson, H. C., Stanford, S. A., & Deharveng, J.-M. 1998, ApJ, 504, 113
Bruzual, G. 2007, in IAU Symp. 241, Stellar Populations as Building Blocks of Galaxies, ed. A. Vazdekis & R. Peletier (Cambridge: Cambridge Univ. Press), 125
Buonanno, R., Corsi, C., Bellazzini, M., Ferraro, F. R., & Pecci, F. F. 1997, AJ, 113, 706
Burstein, D., Bertola, F., Buson, L. M., Faber, S. M., & Lauer, T. R. 1988, ApJ, 328, 440
Buson, L. M., Bertone, E., Buzzoni, A., & Carraro, G. 2006, Baltic Astron., 15, 49
Busso, G., Moehler, S., Zoccali, M., Heber, U., & Yi, S. K. 2005, ApJ, 633, L29
Buzzoni, A. 1989, ApJS, 71, 817
———. 1993, A&A, 275, 433
———. 1995, ApJS, 98, 69
———. 1998, in, T. Zanzu, V. Testa & M. Bellazzini eds., Evolving Evolution (Cagliari: Oss. di Cagliari), 13 (astro-ph/9811382)
———. 2008, in, D. Valls-Gabaud & M. Chavez eds., Resolved Stellar Populations, ASP Conf. Ser. (ASP: San Francisco), in press (astro-ph/0509602)
Buzzoni, A., Arnaboldi, M., & Corradi, R. L. M. 2006, MNRAS, 368, 877
Buzzoni, A., Gariboldi, G., & Mantegazza, L. 1992, AJ, 103, 1814
Buzzoni, A., Mantegazza, L., & Gariboldi, G. 1994, AJ, 107, 513
Cantiello, M., Raimondo, G., Brocato, E., & Capaccioli, M. 2003, AJ, 125, 2783
Castellani, M., Limongi, M., & Tornambé A. 1992, ApJ, 389, 227
Castellani, M., & Tornambé A. 1991, ApJ, 381, 393
Castellani, V., Giannone, P., & Renzini, A. 1970, Ap&SS, 9, 418
Castellani, V., Iannicola, G., Bono, G., Zoccali, M., Cassisi, S., & Buonanno, R. 2006, A&A, 446, 569
Castellani, V., & Renzini, A. 1968, Ap&SS, 2, 310
Catelan, M., Ferraro, F. R., & Rood, R. T. 2001, ApJ, 560, 970
Cerviño, M., & Luridiana, V. 2006, A&A, 451, 475
Cerviño, M., Luridiana, V., & Castander, F. J. 2000, A&A, 360, L5
Cerviño, M., Valls-Gabaud, D., Luridiana, V., & Mas-Hesse, J. M. 2002, A&A, 381, 51
Chabrier, G. 2003, PASP, 115, 763
Charbonnel, C., Meynet, G., Maeder, A., & Schaerer, D. 1996, A&AS, 115, 339
Chiosi, C., Bertelli, G., & Bressan, A. 1992, ARA&A, 30, 235
Code, A. D., & Welch, G. A. 1979, ApJ, 228, 95
Cohen, J. G. 1982, ApJ, 258, 143
Colina, L., Bohlin, R. C., & Castelli, F. 1996, Instrum. Sci. Rep. CAL/SCS-008 (Baltimore: STScI)
Cox, J. P., & Giuli, R. T. 1968, Principles of Stellar Structure (New York: Gordon & Breach)
D'Cruz, N. L., Dorman, B., Rood, R. T., & O'Connell, R. W. 1996, ApJ, 466, 359

D'Cruz, N. L., Morgan, S. M., & Böhm-Vitense, E. 2000, AJ, 120, 990
Demarque, P., Mengel, J. G., & Sweigart, A. V. 1972, ApJ, 173, L27
Demleitner, M., Accomazzi, A., Eichhorn, G., Grant, C. S., Kurtz, M. J., & Murray, S. S. 2001, in ASP Conf. Ser. 238, Astronomical Data Analysis Software and Systems X, ed. F. R. Harnden, Jr. et al. (San Francisco: ASP), 321
de Vaucouleurs, G., de Vaucouleurs, A., Corwin, H. G., Jr., Buta, R. J., Paturel, G., & Fouque, P. 1991, Third Reference Catalog of Bright Galaxies (Heildelberg: Springer)
Dorman, B., Rood, R. T., O'Connell, R. W. 1993, ApJ, 419, 596
Dorman, B., O'Connell, R. W., & Rood, R. T. 1995, ApJ, 442, 105
Ferguson, H. C., & Davidsen, A. F. 1993, ApJ, 408, 92
Frogel, J. A., Mould, J., & Blanco, V. M. 1990, ApJ, 352, 96
Fusi Pecci, & F., & Renzini, A. 1976, A&A, 46, 447
González, R. A., Liu, M. C., & Bruzual, A., G. 2004, ApJ, 611, 270
———. 2005, ApJ, 621, 557
González-López1ira, R. A., Albarrán, M. Y., Mouhcine, M., Liu, M. C., Bruzual-A, G., & de Batz, B. 2005, MNRAS, 363, 1279
Greggio, L., & Renzini, A. 1990, ApJ, 364, 35
Groenewegen, M. A. T., Smith, C. H., Wood, P. R., Omont, A., & Fujiyoshi, T. 1995, ApJ, 449, L119
Hui, X., Ford, H. C., Ciardullo, R., & Jacoby, G. H. 1993, ApJ, 414, 463
Iben, I., Jr., & Renzini, A. 1983, ARA&A, 21, 271
Iben, I., Jr., & Rood, R. T. 1970, ApJ, 161, 587
Jensen, J. B., Luppino, G. A., & Tonry, J. L. 1996, ApJ, 468, 519
Jensen, J. B., Tonry, J. L., Barris, B. J., Thompson, R. I., Liu, M. C., Rieke, M. J., Ajhar, E. A., & Blakeslee, J. P. 2003, ApJ, 583, 712
Jensen, J. B., Tonry, J. L., & Luppino, G. A. 1998, ApJ, 505, 111
Johnson, H. L. 1966, ARA&A, 4, 193
Kaluzny, J., & Udalski, A. 1992, Acta Astron., 42, 29
Kobayashi, C., & Arimoto, N. 1999, ApJ, 527, 573
Kuntschner, H., Lucey, J. R., Smith, R. J., Hudson, M. J., & Davies, R. L. 2001, MNRAS, 323, 615
Larson, R. B. 1974, MNRAS, 166, 585
Lee, M. G., Freedman, W. L., & Madore, B. F. 1993, ApJ, 417, 553
Lee, Y.-W., et al. 2005, ApJ, 619, L103
Liu, M. C., Graham, J. R., & Charlot, S. 2002, ApJ, 564, 216
Maraston, C., Greggio, L., & Thomas, D. 2001, Ap&SS, 276, 893
Marigo, P., & Girardi, L. 2007, A&A, 469, 239
Marigo, P., Girardi, L., Weiss, A., Groenewegen, M. A. T., & Chiosi, C. 2004, A&A, 423, 995
Mateo, M. L. 1998, ARA&A, 36, 435
Mouhcine, M., González, R. A., & Liu, M. C. 2005, MNRAS, 362, 1208
O'Connell, R. W. 1999, ARA&A, 37, 603
Paczyński, B. 1970, Acta Astron., 20, 47
Pahre, M. A., de Carvalho, R. R., & Djorgovski, S. G. 1998, AJ, 116, 1606
Pahre, M. A., & Mould, J. R. 1994, ApJ, 433, 567
Park, J.-H., & Lee, Y.-W. 1997, ApJ, 476, 28
Paturel, G., Petit, C., Prugniel, P., Theureau, G., Rousseau, J., Brouty, M., Dubois, P., & Cambrésy, L. 2003, A&A, 412, 45
Peimbert, M. 1990, Rev. Mex. AA, 20, 119
Persson, S. E., Murphy, D. C., Krzeminski, W., Roth, M., & Rieke, M. J. 1998, AJ, 116, 2475
Piersanti, L., Tornambé, A., & Castellani, V. 2004, MNRAS, 353, 243
Raimondo, G., Brocato, E., Cantiello, M., & Capaccioli, M. 2005, AJ, 130, 2625
Recio-Blanco, A., Aparicio, A., Piotto, G., de Angeli, F., & Djorgovski, S. G. 2006, A&A, 452, 875
Ree, C. H., et al. 2006, Baltic Astron., 15, 5
Reimers, D. 1975, Mem. Soc. R. Sci. Liège, 8, 87
Renzini, A. 1977, in Advanced Stages in Stellar Evolution, ed. I. Iben, Jr., A. Renzini, & D. N. Schramm (Heidelberg: Springer)
———. 2006, ARA&A, 44, 141

Renzini, A., & Buzzoni, A. 1986, in Spectral Evolution of Galaxies, ed. C. Chiosi & A. Renzini (Dordrecht: Reidel), 195
Renzini, A., & Fusi Pecci, F. 1988, ARA&A, 26, 199
Rich, R. M., et al. 1997, ApJ, 484, L25
Rose, J. A., & Deng, S. 1999, AJ, 117, 2213
Schönberner, D. 1983, ApJ, 272, 708
Schiavon, R. P., Caldwell, N., & Rose, J. A. 2004, AJ, 127, 1513
Searle, L., Wilkinson, A., & Bagnuolo, W. G. 1980, ApJ, 239, 803
Seidel, E., Da Costa, G. S., & Demarque, P. 1987, ApJ, 313, 192
Skrutskie, M. F., et al. 1997, in The Impact of Large Scale Near-IR Sky Surveys, ed. F. Garzon et al. (ASSL vol. 210; Dordrecht: Kluwer), 25
Stanghellini, L., & Renzini, A. 2000, ApJ, 542, 308
Sweigart, A. V. 1997, ApJ, 474, L23
Sweigart, A. V., Brown, T. M., Lanz, T., Landsman, W. B., & Hubeny, I. 2002, in ASP Conf. Ser. 265, Omega Centauri, A Unique Window into Astrophysics, ed. F. van Leeuwen, J. D. Hughes, & G. Piotto (San Francisco: ASP), 261
Sweigart, A. V., & Gross, P. G. 1976, ApJS, 32, 367
Tantalo, R., Chiosi, C., Bressan, A., & Fagotto, F. 1996, A&A, 311, 361
Tonry, J. L. 1991, ApJ, 373, L1
Tonry, J., & Schneider, D. P. 1988, AJ, 96, 807
Unglaub, K., & Bues, I. 2001, A&A, 374, 570
van Loon, J. T. 2000, A&A, 354, 125
Worthey, G. 1993, ApJ, 409, 530
———. 1994, ApJS, 95, 107
Yi S., Demarque, P., & Oemler, A. J. 1998, ApJ, 492, 480
Yi, S. K., & Yoon, S.-J. 2004, Ap&SS, 291, 205